Eur. Phys. J. Special Topics **157**, 61–77 (2008)

DOI: 10.1140/epjst/e2008-00631-1

THE EUROPEAN PHYSICAL JOURNAL SPECIAL TOPICS

Beyond the Keller-Segel model

Microscopic modelling of bacterial colonies

P. Romanczuk[1,a], U. Erdmann[2], H. Engel[3], and L. Schimansky-Geier[1]

[1] Institute of Physics, Humboldt University Berlin, Newtonstr. 15, 12489 Berlin, Germany
[2] Helmholtz Association, Anna-Louisa-Karsch-Str. 2, 10178 Berlin, Germany
[3] Institute of Theoretical Physics, Technical University Berlin, Hardenbergstr. 36, 10623 Berlin, Germany

Abstract. Complex spatio-temporal patterns of cell clusters were observed in colonies of chemotactic bacteria such as Escherichia coli or Sallmonella typhimurium. The production of a potent chemoattractant by the bacteria themselves as a reaction to certain nutrients is the essential factor for this pattern formation. Additional collective dynamics, such as collective translation and rotation of bacterial clusters were reported from experiments on bacterial colonies. Motivated by this observations we suggest a simple model for the description of bacterial colonies using the concept of active Brownian particles. Individual based models represent an interesting alternative to the usually employed mean field chemotaxis-diffusion equations (Keller-Segel model) as they allow us to study the macroscopic pattern formation of the colony, the collective dynamics of bacterial ensembles, as well as the microscopic dynamics of individual cells. In this paper we derive microscopic model equations from basic assumptions about bacterial dynamics, discuss the parameter choice by comparison with biological data and analyse the macroscopic and microscopic dynamics of the system. Finally we extend the model by a velocity-alignment (swarming) interaction which leads to novel collective dynamics in the system.

1 Introduction

Bacterial colonies are among the simplest systems in nature and are particularly well suited for the study of self-organisation and pattern formation in biological systems. The driving motivation for such a research from a physicist's point of view is to gain profound insights into the origin of the fascinating complex behaviour as a result of simple microscopic interactions between individual biological agents.

Most models employed for the description of bacterial colonies with chemical cell-to-cell signaling (chemotaxis) are based on the so-called Keller-Segel model (KSM) [1,2]. It is a continuous model of partial differential equations (PDEs) for the dynamics of the bacterial density $\rho(\mathbf{x}, t)$ and the concentration(s) of the involved chemical agent(s) $c(\mathbf{x}, t)$. The mean field approach (KSM) has been employed to describe a wide range of bacterial pattern formation phenomena and has provided good results for macroscopic dynamics of bacterial colonies (see e.g. [3–6]). The downside of the model is its inability to account for active motion of bacteria, the dynamics of single cells and the often numerically demanding procedures for solutions of coupled PDEs. Generally, in dealing with dynamics of bacterial colonies, we encounter structures of relatively few cells and in those cases the continuous description is at least questionable.

[a] e-mail: romanczuk@physik.hu-berlin.de

Motivated by experiments of Budrene & Berg [7,8] we propose in this paper an individual based model for bacterial colonies with chemotaxis. In the first section we derive the microscopic equations taking into account active motility and chemotaxis. The model is closely related to the individual based model introduced by Ben-Jacob et al. [9]. The second section deals with the discussion of the macroscopic pattern formation of our model by a Keller-Segel type mean field description neglecting active motion. After showing the linkage to the classical PDE-approach we will proceed beyond the classical KSM-model with an analysis of the microscopic dynamics. Finally we will introduce an additional microscopic velocity-alignment interaction which leads to novel dynamical behaviour on the macroscopic scale.

2 Bacteria from a physicist point of view

Bacteria as living entities, are not simply obeying basic physical laws but interact with their environment in an active way. A basic feature of a wide number of bacterial species is their ability to explore their environment via active motion.

Most common motility type of bacteria is a movement driven by external organelles, the so-called flagella. The helical flagella rotate and in this way excert thrust that drives the cell. Bacterial swimming velocities range from 10–35 μm/s for rod-shaped cells like *E. coli* and *Salmonella* up to $\approx 200\,\mu$m/s for some species of Marine bacteria [10]. Depending on the number and location of the flagella and the bacterial species various types of flagellar swimming can be observed. Cells of *E.coli* and *Salmonella* move actively in straight runs, that are interrupted by reorientation events, the so-called "tumbling". Effectively the motion of individual bacteria can be described as an random walk combined with a finite swimming velocity.

A mathematical description of active motion in biology can be realized by a general Langevin ansatz for the evolution of the position and the velocity vectors of an individual with mass m in a d-dimensional space ($\mathbf{x}, \mathbf{v} \in \mathbb{R}^d$):

$$\dot{\mathbf{x}} = \mathbf{v} \tag{1a}$$

$$m\dot{\mathbf{v}}(\mathbf{x}, \mathbf{v}, t) = -\gamma(\mathrm{v})\mathbf{v} + \mathbf{F}(\mathbf{x}) + \mathbf{F}^{\mathrm{s}}(t)\ . \tag{1b}$$

The terms on the right hand side of Eq. (1b) are a velocity dependent friction function $\gamma(\mathrm{v})$, an arbitrary external force $\mathbf{F}(\mathbf{x})$ acting on the agent and a stochastic force $\mathbf{F}^{\mathrm{s}}$. The stochastic force is introduced by white noise with the intensity D_v.

$$\langle \mathbf{F}^{\mathrm{s}}(t) \rangle = 0; \quad \langle \mathbf{F}^{\mathrm{s}}(t)\mathbf{F}^{\mathrm{s}}(t') \rangle = 2^d D_v \delta(t - t'). \tag{2}$$

For bacteria swimming with a finite velocity $\mathrm{v}_0 > 0$ a possible choice for $\gamma(\mathrm{v})$ is the non-linear Rayleigh-type friction function:

$$\gamma(\mathrm{v}) = -\gamma_1 + \gamma_2 \mathrm{v}^2, \qquad \gamma_2 > 0\ . \tag{3}$$

It can be derived from a minimal model for animal motion introduced by Ebeling et al. [11] and was studied in detail in [12–14]. The stationary velocity distribution for the Rayleigh ansatz in the absence of external forces $\mathbf{F}(\mathbf{x})$ can be obtained via the Fokker-Planck equation (m = 1),

$$\frac{\partial P(\mathbf{v})}{\partial t} = \frac{\partial}{\partial \mathbf{v}} \left(\gamma(\mathbf{v})\mathbf{v}P + D_v \frac{\partial P}{\partial \mathbf{v}} \right), \tag{4}$$

and reads:

$$P^0(\mathbf{v}) \propto \exp\left(\frac{\gamma_1}{2D_v}\mathbf{v}^2 - \frac{\gamma_2}{4D_v}\mathbf{v}^4 \right). \tag{5}$$

For $\gamma_1 \leq 0$ the maximum of the distribution is located at $\mathbf{v} = 0$. For $\gamma_1 > 0$, the mean velocity is still zero, but the maxima of the distribution shift to a finite value. The particles are most likely to move with a finite velocity $\mathbf{v}_0^2 = \gamma_1/\gamma_2$.

Essential for the survival of microorganisms in general, and bacteria in particular, is their ability to move towards beneficial environments and away from hostile environments. In order to find these favorable conditions bacteria are capable of temporal sensing of concentration differences of different chemical agents via specialized membrane receptors. This feature coupled together with the ability to bias their movement towards higher concentrations of certain substances, so-called chemoattractants, or away from certain chemicals, so-called chemorepellents, is called chemotaxis [10]. Chemotaxis depends on complex intracellular processes and is the subject of ongoing research (see e.g. [15–17]).

For our purpose, we introduce chemotaxis as an effective force $\mathbf{F}_{\mathrm{ch}}$ acting on an individual bacterium and leading to an effective drift into the direction of the chemoattractant gradient:

$$\mathbf{F}_{\mathrm{ch}} = \kappa(c)\nabla c, \tag{6}$$

where c is the concentration of the respective chemical and $\kappa(c)$ is the chemotactic response, or sensitivity, function, which in general depends on the concentration of the chemical itself.

Bacteria sense the local concentration gradient of chemicals via the temporal comparison of the relative occupation of their membrane receptors $R = N_o/(N_o + N_f)$, where N_o and N_f is the number of occupied receptors and free receptors, respectively.

If we assume that these numbers are determined by the time constants of the mean occupation time τ_o and the mean free time of a receptor τ_f, and use $\tau_f \sim c^{-1}$, we can write R as a function of the concentration of the chemical (see Ref. [18]):

$$R = \frac{N_o}{N_f + N_o} = \frac{\tau_o}{\tau_f + \tau_o} = \frac{c}{a + c} \tag{7}$$

where $a \equiv (c\tau_f)/\tau_o$ is a constant. The temporal sensing of the relative occupation R combined with a finite stationary velocity v_0 leads to an effective measurement of spatial gradients of the relative occupation of membrane receptors R. Hence we introduce a chemotactic force acting on individual cells that is proportional to the spatial gradient of relative occupation of its receptors R:

$$\mathbf{F}_{\mathrm{ch}} \propto \nabla R. \tag{8}$$

Assuming τ_o to be spatially constant in Eq. (7) and rescaling the constants we formulate the chemotactic force as

$$\mathbf{F}_{\mathrm{ch}} = \frac{\kappa_0}{(1 + \beta c)^2}\nabla c, \tag{9}$$

where κ_0 is the chemotactic sensitivity coefficient which is positive for chemoattractants and negative for chemorepellents. The second parameter β is a constant characterizing the saturation of the membrane receptors. The resulting expression for $\kappa(c)$ from comparison of Eq. (6) and Eq. (9) is equivalent to the chemotactic receptor law in [19].

A common situation in bacterial dynamics is that the respective chemoattractant (chemorepellent) is produced by the bacteria themselves. This is considered as chemical cell to cell signaling. By these means bacteria are able to exchange information about favorable or disadvantageous environmental conditions.

The dynamics of the chemoattractant (or chemorepellent) obey a simple reaction diffusion equation:

$$\frac{\partial c(\mathbf{x}, t)}{\partial t} = Q(\mathbf{x}, t) + d_c c(\mathbf{x}, t) + D_c \Delta c(\mathbf{x}, t), \tag{10}$$

where c is the concentration, Q the production rate, d_c the decay rate, and D_c the diffusion coefficient of the respective chemoattractant (chemorepellent).

3 Active Brownian particles with chemotaxis

We describe a colony of bacteria interacting via a self-generated chemoattractant, by a set of N active particles. Each particle represents, depending on the particular problem, either an

individual cell or a small ensemble of bacteria (10–1000 cells). Such an ensemble approach is only justified if the length scale of the interaction is much larger than the size of the ensemble represented by a single particle and was previously employed and tested in individual based model for bacterial dynamics by Czirók et al. [9].

Thus we formulate the following model for N active particles ($i = 1 \dots N$):

$$\dot{\mathbf{x}}_i = \mathbf{v}_i \tag{11a}$$

$$m_i \dot{\mathbf{v}}_i = (\gamma_1 - \gamma_2 \mathbf{v}_i^2)\mathbf{v}_i + \frac{\kappa_0}{(1 + \beta c(\mathbf{x}_i))^2} \nabla c(\mathbf{x}_i) + \mathbf{F}_i^s(t) \tag{11b}$$

$$\dot{c} = q_0 \sum_{i=1}^{N} \delta(\mathbf{x} - \mathbf{x}_i) - d_c c(\mathbf{x}, t) + D_c \Delta c(\mathbf{x}, t). \tag{11c}$$

In general bacterial dynamics take place in a three dimensional space but in most experimental set-ups we deal effectively with 2d-systems of thin bacterial films in a petri dish. Therefore we will restrict ourselves in the analysis of the above model equations (11) to the two dimensional case ($d = 2$).

If we neglect the c-dependence of the chemotactic response $\beta = 0$ and replace the Rayleigh friction function by a constant friction $-\gamma_0$ we obtain a model previously studied by Schweitzer & Schimansky-Geier (SSG-model) [20].

Depending on the model parameters they observed formation of spike patterns of the chemoattractant field c. The spikes correspond to particle clusters agglomerating at high concentration of c. The positive feedback between the spike "height" and attraction on other particles leads to a competition between spikes following an Eigen-Fisher like dynamics. After a certain relaxation time only few spikes "survive", but even if the dynamics of the system slows down, in the limiting case of $t \to \infty$ the only stationary solution is a single spike of the chemical field or cluster of particles, respectively. This process can be seen as an Ostwald-ripening process known from chemical reactions.

The macroscopic behavior of our model is similar to that observed in the SSG-model with some important differences: Due to the finite stationary particle velocity and the saturation of the chemotactic sensitivity also additional dynamical behavior can be observed.

The decrease of the chemotactic force at high concentrations c for $\beta > 0$, makes particles insensitive towards the gradient of c—the particles are able to leave the maxima of the field distribution. This behavior has significant impact on the macroscopic pattern formation as compared to the SSG-model. At large β any formation of clusters may be inhibited and at moderate values of β a "smoothing" of spikes in the concentration profile towards flat spots can be observed (see Fig. 1).

Finally due to the active motion of particles with a finite stationary velocity we deal with a system of confined self-propelled particles. The particles move in self-generated dynamical potential landscape. An analysis of the microscopic dynamics is given in section 4.

3.1 Reduction of free parameters

By applying the above model to bacterial dynamics it is possible to reduce the number of free parameters by taking into account biological data.

The stationary velocity of bacteria eliminates one of the two parameters of the Rayleigh-friction: $\gamma_2 = \gamma_1 / {v_0}^2$. Considering the fact that the bacterial dynamics take place in a extremely low Reynolds number environment, $Re \approx 10^{-6}$, we get an additional condition restricting the choice on the respective parameters: $\gamma_1 \ll \gamma_2$.

An experimentally accessible quantity of bacterial dynamics is the mean square displacement which for pure Brownian motion increases linearly in time:

$$\left\langle (\mathbf{x} - \mathbf{x}_0)^2 \right\rangle (t) = 2^d D t. \tag{12}$$

Here, D is the ordinary diffusion coefficient and d again the spatial dimension.

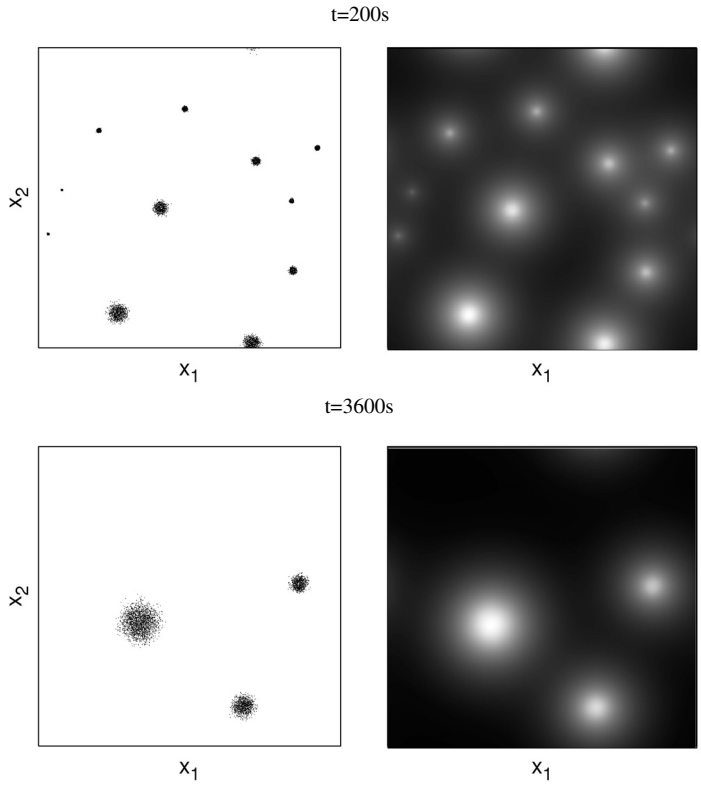

Fig. 1. Evolution of a system of Active Brownian particles with homogenous distribution of particles and $c(\mathbf{x}) = 0$ (left: particle positions as single points; right: the chemoattractant field c as a concentration plot—bright areas correspond to high c-concentration). After an initial fast formation of a large number of small clusters (top) fusion and growth of clusters takes place until a quasi-stationary state of few large clusters is reached (bottom). In the long time limit $t \to \infty$ these few cluster should fuse and form a single extended cluster (Ostwald-ripening).

In the case of active Brownian motion it was shown in [21] that for $d = 2$ and vanishing fluctuations of the velocity magnitude $\mathrm{v}(t) \approx \mathrm{v}_0$ the mean square displacement grows approximately in time as:

$$\left\langle (\mathbf{x}(t) - \mathbf{x}_0)^2 \right\rangle = \frac{2\mathrm{v}_0^4}{D_v} t \tag{13}$$

The comparison with the ordinary Brownian motion leads to spatial diffusion process with an effective diffusion coefficient $\hat{D}(\mathrm{v}_0, D_v)$:

$$\hat{D} = \frac{v_0^4}{2D_v} = \frac{\gamma_1^2}{2D_v\gamma_2^2}. \tag{14}$$

Eq. (14) determines the noise intensity D_v for given γ_1, γ_2 and $\hat{D}$.

As the approximation for the effective spatial diffusion coefficient $\hat{D}$ (Eq. (14)) breaks down for our choice of γ_1 and γ_2 (see Table 1) we determined D_v via the mean square displacement obtained from numerical calculations of Eq. (1) for $\mathbf{F} = 0$.

The effective diffusion coefficient $\hat{D}$ of bacteria, as well as, the spatial diffusion coefficient for the chemoattractant D_c can be obtained from experimental data (see Table 1).

The bacterial mass m may also be obtained from experimental data, but the reported values vary several order of magnitude depending on the species and the growth conditions [22]. For

Table 1. Biological data on bacterial colonies and the parameters used in all numerical simulations for d = 2 if not stated otherwise.

biologically data	numerical parameters (d = 2)
velocity of individual bacteria $\approx 0.02\,\mathrm{mm/s}$ [10]	$\gamma_1 = 4.0\,\frac{1}{\mathrm{s}}$, $\gamma_2 = 10^4\,\frac{\mathrm{s}}{\mathrm{mm}^2}$
diffusion coefficient of the chemoattractant $\approx 10^{-3}\,\mathrm{mm}^2/\mathrm{s}$ [8]	$D_c = 10^{-3}\,\mathrm{mm}^2\,\mathrm{s}^{-1}$
effective diffusion coefficient of bacteria $\hat{D} \approx 5 \cdot 10^{-4}\,\mathrm{mm}^2/\mathrm{s}$ [8]	$D_v = 1 \times 10^{-4}\,\mathrm{mm}^2\,\mathrm{s}^{-3}$
bacterial mass $\approx 10^{-15} - 10^{-18}\,\mathrm{kg}$ [22]	$m = 1$ a.u.
chemoattractant production rate	$q_0 = 1$ a.u.

simplicity we set the bacterial mass to unity ($m = 1$) in the following analysis. Therefore all forces are rescaled by the bacterial mass.

Finally, we set in most simulations the chemoattractant production rate q_0 to unity ($q_0 = 1$). In this case the chemoattractant concentrations c is given in units of chemoattractant produced per bacterium per second.

Through the usage of biological data and rescaling of the equations we are able to reduce the free parameters down to three: the chemotactic sensitivity κ_0, the chemotactic saturation coefficient β and the chemoattractant decay rate d_c. The fixed parameters used in numerical simulations are summarize in Table 1.

3.2 Macroscopic pattern formation

In this section we address two questions: 1) Does active motility alter the macroscopic dynamics? 2) What impact do the macroscopic parameters κ_0, β and d_c have on the macroscopic pattern formation?

For the study of pattern formation we neglect the microscopic feature of active motion and consider the particles to behave as normal Brownian particles with a constant friction normalized by the particle mass $\gamma(\mathbf{v}_i)/m = \gamma_0 = const.$ This approach can be justified by the small stationary velocity of bacteria. With this assumption and in the overdamped limit (Smoluchowski limit) the dynamics of (11) reduce to ($m = 1$):

$$\dot{\mathbf{x}}_i = \frac{\kappa_0}{\gamma_0(1+\beta c)^2}\nabla c + \frac{1}{\gamma_0}\mathbf{F}_i^s(t) \tag{15a}$$

$$\dot{c} = q_0 \sum_{i=1}^{N} \delta(\mathbf{x} - \mathbf{x}_i) - d_c c + D_c \Delta c. \tag{15b}$$

From Eq. (15a) we can derive via the corresponding Fokker-Planck equation an equation for the evolution of the particle density ρ. We end up with a set of PDEs, that represents a reactions-diffusion system with chemotaxis and can be seen as a particular realization of the Keller-Segel model which corresponds to our microscopic model. A similar system has been studied by

Tyson et al. [3,4]:

$$\dot{\rho}(\mathbf{x},t) = \nabla\left(-\frac{\kappa_0\rho}{\gamma_0(1+\beta c)^2}\nabla c + D\nabla\rho\right), \tag{16a}$$

$$\dot{c} = q_0\rho - d_c c + D_c\Delta c. \tag{16b}$$

Here, $D = D_v/\gamma_0^2$ is the spatial diffusion coefficient of the overdamped dynamics. The simplest stationary solution of (16) is the homogeneous solution, given by the average densities:

$$\rho_{\text{hom}} = \frac{N}{A} = \bar{\rho}, \qquad N = \int_A \rho(\mathbf{x},t)d\mathbf{x}, \tag{17a}$$

$$c_{\text{hom}} = \frac{C}{A} = \bar{c}, \qquad C = \int_A c(\mathbf{x},t)d\mathbf{x}. \tag{17b}$$

We consider a periodic boundary condition, so that effectively we deal with a closed system where the diffusion processes do not change the total amount of the chemoattractant within the system. The total amount of chemoattractant obeys the following differential equation:

$$\frac{dC}{dt} = -d_c C + q_0 N, \tag{18}$$

with the initial conditions $C(t=0) = 0$ and $d_c > 0$ the solution of (18), is given by

$$C(t) = \frac{q_0}{d_c}N(1 - e^{-d_c t}) \overset{t\to\infty}{\longrightarrow} \frac{q_0}{d_c}N, \tag{19}$$

and for vanishing chemoattractant decay $d_c = 0$ it is given by

$$C(t) = q_0 N t. \tag{20}$$

For $d_c = 0$ the total amount of the chemoattractant C increases linearly with time. For $d_c > 0$ it approaches asymptotically a constant level $q_0/d_c N$ and after the time $t = \tau = 5/d_c$ it reaches 99% of the final amount. Therefore the homogeneous solution c_0 for $t \gg \tau$ is

$$\bar{c} = \frac{q_0}{d_c}\bar{\rho} \tag{21}$$

for $d_c > 0$, and

$$\bar{c}(t) = q_0\bar{\rho}t \tag{22}$$

for $d_c = 0$.

Let us now analyze the stability of homogeneous stationary solution given by (17). We allow for small perturbations around $\bar{\rho}$ and $\bar{c}$:

$$\begin{aligned}\rho(\mathbf{x},t) &= \bar{\rho} + \delta\rho, \ \text{ with } \ \delta\rho = \epsilon\sum_k f_{\mathbf{k}}(t)e^{-i\mathbf{k}\mathbf{x}},\\ c(\mathbf{x},t) &= \bar{c} + \delta c, \ \text{ with } \ \delta c = \epsilon\sum_k g_{\mathbf{k}}(t)e^{-i\mathbf{k}\mathbf{x}},\end{aligned} \tag{23}$$

with $f_{\mathbf{k}}$, $g_{\mathbf{k}}$ as the Fourier amplitudes for the wave vector $\mathbf{k}$ of the perturbation and $\epsilon \ll 1$.

Inserting (23) in (16) and linearization in ϵ leads to a set of differential equations for the evolution of the particular Fourier amplitudes $f_{\mathbf{k}}$, $g_{\mathbf{k}}$. The coupled first order differential equations can be combined to a second order differential equation for either of the Fourier amplitudes, e.g., for the field perturbation $g_{\mathbf{k}}$:

$$\frac{d^2 g_{\mathbf{k}}}{dt^2} + \Big((D_c + D)\mathbf{k} + d_c\Big)\frac{dg_{\mathbf{k}}}{dt} + \left(DD_c\mathbf{k}^2 + Dd_c - \frac{\kappa_0\bar{\rho}q_0}{\gamma_0(1+\beta\bar{c})^2}\right)\mathbf{k}^2 g_{\mathbf{k}} = 0. \tag{24}$$

For vanishing chemoattractant decay $d_c = 0$ we have a continuous accumulation of chemoattractant in the system ($\bar{c} \to \infty$ as $t \to \infty$). It can be easily shown that in this case and for finite chemotactic saturation coefficient $\beta > 0$ only the homogenous solution is asymptotically stable.

For finite chemoattractant decay $d_c > 0$ we can substitute $\bar{c}$ according to (21) and obtain a differential equation with constant coefficients that can be solved by a $g_{\mathbf{k}} \sim e^{\lambda t}$ ansatz with the solutions:

$$\lambda_{+/-} = -\frac{\left((D_c + D)\mathbf{k}^2 + d_c\right)}{2} \pm \sqrt{\frac{\left((D_c + D)\mathbf{k}^2 + d_c\right)^2}{4} - \left(DD_c\mathbf{k}^2 + Dd_c - \frac{\kappa_0 \bar{\rho} q_0}{\gamma_0 (1 + \beta \frac{q_0}{d_c}\bar{\rho})^2}\right)\mathbf{k}^2}. \tag{25}$$

For homogeneous fluctuations of ρ and c with $\mathbf{k} = 0$ we get

$$\lambda_- = -d_c, \quad \lambda_+ = 0. \tag{26}$$

This reflects the conservation of the number of particles N and the stability of the c-field for this case. For finite $\mathbf{k}$-vectors (inhomogeneous fluctuations) the homogeneous solution is stable as long as the following relationship holds:

$$\left(DD_c\mathbf{k}^2 + Dd_c - \frac{\kappa_0 \bar{\rho} q_0}{\gamma_0 (1 + \beta \frac{q_0}{d_c}\bar{\rho})^2}\right) \geq 0, \tag{27}$$

or alternatively for the chemotactic sensitivity κ_0:

$$\kappa_0 \leq \frac{D\gamma_0}{\bar{\rho} q_0}(D_c\mathbf{k}^2 + d_c)\left(1 + \beta\frac{q_0}{d_c}\bar{\rho}\right)^2. \tag{28}$$

In the long wavelength limit ($\mathbf{k} \to 0$) we end up with an expression for the minimal κ_0 where the condition (27) is fulfilled:

$$\kappa_0 \leq \frac{D\gamma_0 d_c}{\bar{\rho} q_0}\left(1 + \beta\frac{q_0}{d_c}\bar{\rho}\right)^2 = \kappa_c. \tag{29}$$

For $d_c > 0$ and κ_0 smaller than the critical sensitivity κ_c all fluctuations around the homogeneous state decay exponentially. Only if $\kappa_0 \geq \kappa_c$ we expect to see any pattern formation on the macroscopic scale in our system.

This prediction was tested by numerical simulations of the active Brownian particle model for different values of the chemotactic coefficients (κ_0, β). By using the unknown friction coefficient γ_0 as a fit parameter in (29) an excellent agreement between the theory and simulation can be observed (see left Fig. 2). This shows that on the level of macroscopic pattern formation the active motility of individual cells can indeed be neglected as implicitly done by describing bacterial colonies by Keller-Segel-type of equations.

In the next section we will now proceed to the analysis of the microscopic dynamics of individual cells within a chemotactic cluster. This lies beyond the descriptive power of the mean-field approach and we have to return to the microscopic description.

4 Microscopic dynamics

We will now analyze the microscopic behaviour of individual particles within chemotactic clusters. There has been various studies of confined self-propelled particles, but in most cases the

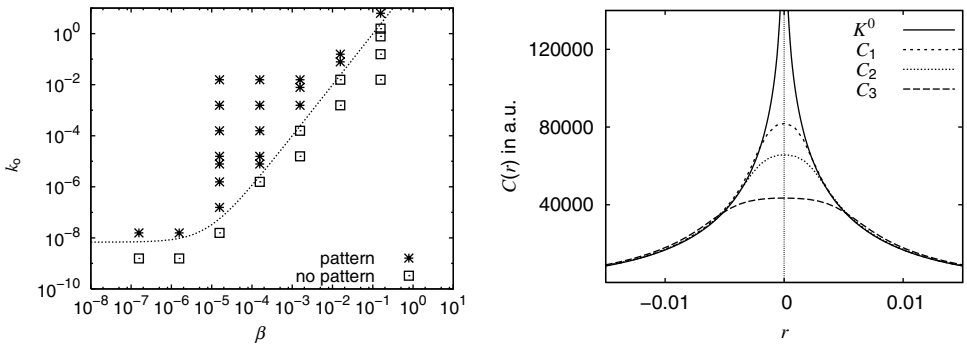

Fig. 2. Left: pattern formation for a system of active Brownian particles in dependence of the chemotactic parameters κ_0 and β. The dashed line represents $\kappa_c(\beta)$ obtained from overdamped limit approximation given in Eq. (29) with $\gamma_0 = 1.7$. Right: stationary field c_s of a single cluster of particles for different values of the saturation coefficient $\beta_1{=}4\times10^{-5}$, $\beta_2 = 5\times10^{-5}$ and $\beta_3 = 7\times10^{-5}$. An increase in β leads to a deviation form the δ-like profile and the corresponding analytical solution $K^0(Ar)$ (34).

considered confinement was either due to reflecting boundary conditions or simple interaction potentials (see e.g.[13,23,24]). In the case of bacteria interacting chemotactically, we deal in general with a dynamic confinement, due to the self-generated chemoattractant profile. The essential dynamics can be well understood by simplification of the potential landscape resulting from the stationary chemoattractant profile.

If the system reaches a stationary state with a stationary chemoattractant profile $c_\mathrm{s}(\mathbf{x})$ (e.g. a single cluster of particles), the individual particle dynamics reads as ($m = 1$):

$$\dot{\mathbf{v}} = (\gamma_1 + \gamma_2\mathbf{v}^2)\mathbf{v} - \nabla C + \sqrt{2D_v}\boldsymbol{\xi} \tag{30}$$

with

$$C(\mathbf{x}) = \frac{\kappa_0}{\beta + \beta^2 c_\mathrm{s}(\mathbf{x})} - \frac{\kappa_0}{\beta}\ . \tag{31}$$

The chemotactic potential C is equivalent to the relative occupation of membrane receptors R (Eq. (7)) and satisfies $C(\mathbf{x}) = 0$ for $c_\mathrm{s}(x) = 0$.

Formally the stationary solution $c_\mathrm{s}(x)$ can be calculated in terms of the Green's function for the chemoattractant diffusion equation in two dimensions

$$G(\mathbf{x}, \mathbf{x'}, t, t') = \frac{q_0}{4\pi D_c(t-t')} \exp\left[\frac{-(\mathbf{x}-\mathbf{x'})^2}{4D_c(t-t')} - d_c(t-t')\right], \tag{32}$$

and the distribution of the particles ρ:

$$c_\mathrm{s}(\mathbf{x}) = \int d\mathbf{x'} \int_{t_0}^{t} dt' G(\mathbf{x}, \mathbf{x'}, t, t')\rho(\mathbf{x'}, t') \tag{33}$$

for $t_0 \to -\infty$. Due to the complex nature of the considered system it is in general not possible to obtain an analytical solution.

For fast relaxation of the particle density $\dot{\rho} \approx 0$, we may simplify (33) by replacing $\rho(\mathbf{x'}, t')$ by stationary density distribution $\rho_\mathrm{s}(\mathbf{x'})$. In most cases (sufficiently large chemoattractant diffusion) rotational symmetry of chemotactic clusters can be assumed (Fig. 1). The chemoattractant profile within a single cluster depends only on the radial distance $r = \sqrt{\mathbf{x}^2 - \mathbf{x}_0^2}$ from the center of the cluster $\mathbf{x}_0$.

For the idealized case of a δ-distribution of particles producing the chemoattractant the stationary solution can be calculated to:

$$c_\mathrm{s}(r) = \frac{q_0 N}{2\pi D_c} K^0(-Ar) \text{ with } A = \frac{d_c}{D_c}\ , \tag{34}$$

Hereby K^0 is the modified Bessel function of the second kind with a singularity at $r = 0$. This solution can be seen as the limiting case of large chemotactic coupling ($\kappa_0 \to \infty$ and $\beta \to 0$), where most particles are strongly confined. It offers a good approximation for for the stationary field c_s and the resulting potential C at finite values of the chemotactic coefficients for $r \gg 0$ but fails to describe c_s at $r \approx 0$ (Fig. 2).

The numerically obtained stationary solutions c_s have a maximum c_max at $r = 0$. Therefore a more reasonable approximation of C can be achieved by a simple parabolic potential $U(r)$:

$$U(r) = \frac{\omega_0^2}{2} r^2 + U_0, \tag{35}$$

with

$$\omega_0^2 = \frac{\kappa_0 S}{(1 + \beta c_\mathrm{max})^2} \tag{36}$$

$$U_0 = -\frac{\kappa_0}{\beta + \beta^2 c_\mathrm{max}} \tag{37}$$

where $S = c''(r = 0)$ is the curvature of the chemoattractant profile at the maximum.

In the framework of our model and with the above approximation a bacterium moving in a chemotactic cluster can be seen as an two dimensional stochastic Rayleigh oscillator [13]:

$$\dot{\mathbf{v}} = (\gamma_1 + \gamma_2 \mathbf{v}^2)\mathbf{v} - \nabla U(r) + \mathbf{F}^\mathrm{s}. \tag{38}$$

For the analysis of (38) in two dimensions we transform our system from Cartesian coordinates $\{\mathrm{x}_1, \mathrm{x}_2, \mathrm{v}_1, \mathrm{v}_2\}$ to polar coordinates $\{r, \psi, v, \phi\}$:

$$\mathbf{x}(t) = \begin{pmatrix} \mathrm{x}_1 \\ \mathrm{x}_2 \end{pmatrix} = r(t) \begin{pmatrix} \sin\psi(t) \\ \cos\psi(t) \end{pmatrix} \tag{39}$$

$$\mathbf{v}(t) = \begin{pmatrix} \mathrm{v}_1 \\ \mathrm{v}_2 \end{pmatrix} = v(t) \begin{pmatrix} \sin\phi(t) \\ \cos\phi(t) \end{pmatrix}. \tag{40}$$

This leads us to the following system of equations of motion for r, ψ, v, ϕ for a particle in a parabolic potential:

$$\dot{r} = v\cos\theta \tag{41a}$$

$$\dot{\psi} = \frac{v}{r}\sin\theta \tag{41b}$$

$$\dot{v} = (\gamma_1 - \gamma_2 v^2)v - \omega_0^2 r_i \cos\theta + \xi_v \tag{41c}$$

$$\dot{\phi} = \frac{1}{v}(\omega_0^2 r \sin\theta + \xi_\phi) \tag{41d}$$

with $\theta = \psi - \phi$.

The noise terms read as

$$\xi_v = \mathrm{F}_\mathrm{x}^\mathrm{s}\cos\phi + \mathrm{F}_\mathrm{y}^\mathrm{s}\sin\phi \tag{42a}$$

$$\xi_\phi = -\mathrm{F}_\mathrm{x}^\mathrm{s}\sin\phi + \mathrm{F}_\mathrm{y}^\mathrm{s}\cos\phi. \tag{42b}$$

Using the properties of the stochastic force $\mathbf{F}^\mathrm{s}$ (2) we obtain

$$\langle\xi_v\rangle = \langle\xi_\phi\rangle = \langle\xi_v\xi_\phi\rangle = 0; \quad \langle\xi_v\xi_{v'}\rangle = \langle\xi_\phi\xi_{\phi'}\rangle = 2D_v. \tag{43}$$

The analysis of a two dimensional deterministic Rayleigh-oscillator ($D_v = 0$) reveals the existence of limit cycles corresponding to rotational motion of particles in either clockwise or counterclockwise direction [25] with $\theta = \pm\pi/2$. The limit cycle energy is

$$\frac{v^2}{2} + \frac{\omega_0^2 r^2}{2} = E_\mathrm{tot}. \tag{44}$$

Assuming that the average potential energy is equal or close to the kinetic energy $\langle E_{\rm pot}\rangle \approx \langle E_{\rm kin}\rangle$ the total energy can be calculated to $E_{\rm tot} = \gamma_1/\gamma_2$. The introduction of noise leads to a smearing out of the deterministic limit cycles and noise induced transitions between the clockwise and counterclockwise rotation. So far only approximate expressions for the stationary distribution in the four-dimensional phase space were found [26,27].

In order to obtain a simple approximate distribution of the radii, we assume that our dynamics deviate only slightly from the limit cycle. Therefore we set $\theta = \pm\pi/2$ in Eqs. (41) and are able to formulate the corresponding Fokker-Planck-Equation for the distribution of the stochastic variable v and ϕ:

$$\frac{\partial P(v,\phi)}{\partial t} = -\frac{\partial}{\partial v}\left\{(\gamma_1 v - \gamma_2 v^3)P\right\} - \frac{\partial}{\partial \phi}\left\{-\frac{\omega_0 r}{v}P\right\} + D_v\frac{\partial^2 P}{\partial v^2} + \frac{D_v}{v^2}\frac{\partial^2 P}{\partial \phi^2}. \tag{45}$$

Integration over ϕ for the stationary case $\partial P/\partial t = 0$ leads us to an equation for the stationary distribution $\tilde{P}^0(v)$ depending only on the velocity, which can be obtained by solving

$$-\frac{\partial}{\partial v}\left\{(\gamma_1 v - \gamma_2 v^3)\tilde{P}\right\} + D_v\frac{\partial^2 \tilde{P}}{\partial v^2} = 0 \tag{46}$$

and reads

$$\tilde{P}^0(v) \propto v\exp\left\{\frac{\gamma_1 v^2}{2D_v} - \frac{\gamma_2 v^4}{4D_v}\right\}. \tag{47}$$

The stationary distribution $\tilde{P}^0(v)$ corresponds to the stationary distribution of a free particle (see Eq. (5)) in polar coordinates. This result is in agreement with our ansatz assuming the motion of the particle being perpendicular to the potential gradient at all times.

If we now use the fact that for perfect rotational motion in a harmonic potential each velocity v corresponds to a certain radial distance r according to

$$r = \frac{v}{\omega_0} \tag{48}$$

we can easily derive an expression for the stationary distribution of the radii:

$$\hat{P}^0(r) \propto \omega_0 r\exp\left\{\frac{\gamma_1\omega_0^2 r^2}{2D_v} - \frac{\gamma_2\omega_0^4 r^4}{4D_v}\right\}. \tag{49}$$

An increase in the chemotactic saturation coefficient β leads to a flattening of the resulting chemotactic potential C. In the harmonic approximation this is equivalent to an increase in the width of the parabolic potential

$$\omega_0(\beta_1) < \omega_0(\beta_2) \qquad \text{for} \qquad \beta_1 > \beta_2. \tag{50}$$

The comparison of the harmonic approximation for the distribution of radii $\hat{P}^0$ (49) with the distribution of particles within a chemotactic cluster P_c obtained from simulations for different values of β shows the same qualitative behaviour: a broadening of the distribution combined with shift towards larger radii (Fig. 3). But in quantitative terms there is systematic shift of P_c to smaller radii in respect to $\hat{P}^0$. This deviation can be easily understood by analyzing the actual particle trajectories as shown in Fig. 4. Due to the stochastic force we observe, additionally to rotational motion, also transient oscillatory motion resulting in an increased probability of smaller radii as the particles cross through the center of the cluster.

Concluding it can be said that the interaction of a large number of self-propelled particles via the self-generated chemoattractant field leads to complex rotational motion of individual particles in an effective potential. It is important to point out that in the simple model equations studied so far (11) the individual particle dynamics within a chemotactic cluster are uncorrelated. Each individual particle performs complex rotational motion with a finite mean angular momentum $L_i > 0$ but the mean momentum over an entire cluster vanishes $\langle L\rangle = \langle\sum_i L_i\rangle \approx 0$ (comp. Eq. (55)). The situation changes on introduction of additional symmetry breaking interaction as presented in the next section.

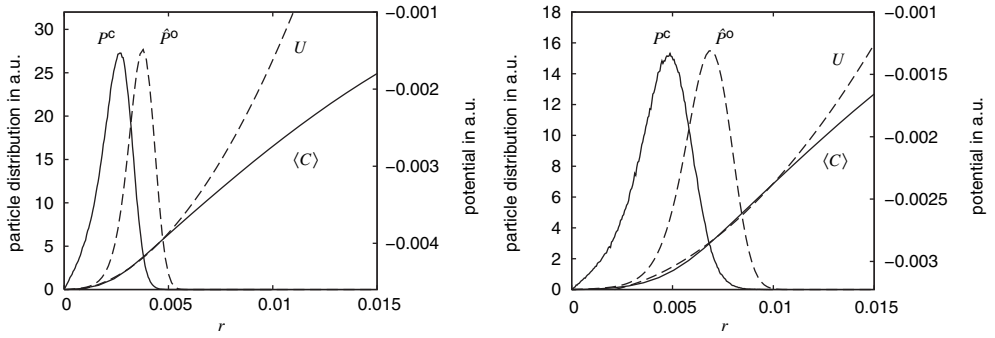

Fig. 3. Comparison of the radial distribution of particles within a chemotactic cluster P^c and the corresponding mean chemotactic potential $\langle C \rangle$ (solid lines) with the stationary distribution from the harmonic approximation $\hat{P}^0$ given in Eq. (49) and the corresponding fit potential U (dashed lines) given in Eq. (35) for $\beta = 5 \times 10^{-5}$ (left) and $\beta = 7 \times 10^{-5}$ (right). (Simulation parameters: $\kappa_0 = 3 \times 10^{-7}$, $N = 4000.$, $q_0 = 0.25$ and $d_c = 10.$)

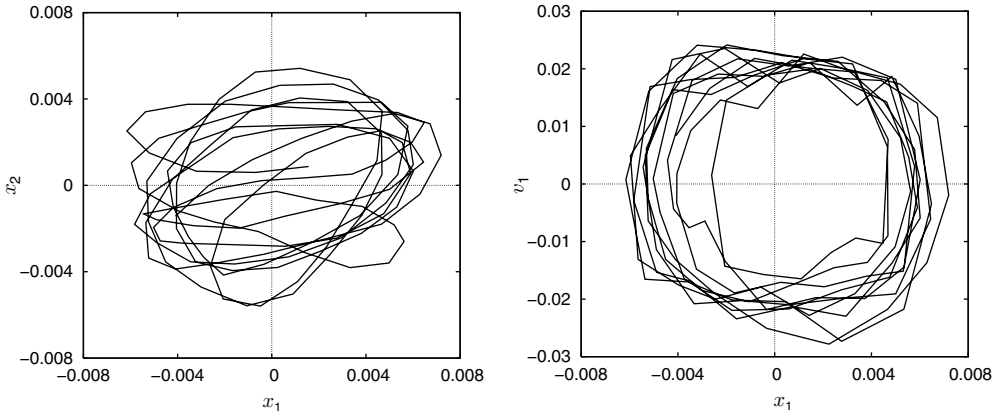

Fig. 4. Projections of the four-dimensional phase space on two dimensional subspaces $\{x_1, x_2\}$ and $\{x_1, v_1\}$. The trajectories of an individual particle within a chemotactic cluster in the x_1x_2-plane deviate significantly from pure rotational motion and show transient oscillatory behaviour (left). The trajectory in the x_1v_1-plane corresponds to noisy limit cycle oscillations (right). (Simulation parameters: $\beta = 7 \times 10^{-5}\,\mathrm{mm}^2$, $\kappa_0 = 3 \times 10^{-7}\,\mathrm{mm}^4\,\mathrm{s}^{-2}$, $N = 4000$, $q_0 = 0.25\,\mathrm{s}^{-1}$ and $d_c = 10\,\mathrm{s}^{-1}$.)

5 Swarming bacteria–from individual dynamics to collective motion

An important feature of bacteria not considered so far in our model is the so-called swarming motility. At certain conditions (e.g. high density, hard surface) a transition from individual swimming behavior to collective dynamics of whole cell ensembles can be observed. In general such a collective dynamics can be accounted for by the introduction of an additional interaction leading to the alignment of the individual particle velocities.

We identify two major mechanisms which may be responsible for velocity-alignment in bacterial dynamics (*E.coli*). The first one is the differentiation of bacteria into filamentous, multi-flagelled swarmer cells. The numerous flagellas lead to a direct coupling of individual cells within a small interaction radius ε. In order to account for the observed behavior we introduce the velocity-alignment force acting on individual cells moving with the velocity $\mathbf{v}_i$ as:

$$\mathbf{F}_{\mathrm{va},i} = \chi(\langle \mathbf{v} \rangle_{\varepsilon,i} - \mathbf{v}_i) \ , \tag{51}$$

$\langle \mathbf{v} \rangle_{\varepsilon,i}$ is the mean velocity of particles within the interaction radius ε of i-th particle and χ is the coupling strength. A reasonable choice of ε is in the order of magnitude of an individual cell size ($\approx 1 - 10\,\mu\mathrm{m}$).

Another interaction that may lead to collective behaviour is a hydrodynamic coupling through the liquid medium at low Reynold numbers. The bacteria feel the mean flow velocity $\mathbf{v}_F$ generated by the motion of their neighbours. The fluid flow at $\mathbf{r}_i$ induced by a point force $\mathbf{F}_j$ acting on the fluid at position $\mathbf{r}_j$ can be written in terms of a hydrodynamic tensor $\mathbf{H}_{ij}$ and the hydrodynamic coupling strength χ_H which is determined by the Stokes friction.

$$\mathbf{v}_F(\mathbf{r}_i) = \chi_H \mathbf{H}_{ij} \mathbf{f}_j. \tag{52}$$

The simplest hydrodynamic tensor, is the so-called Oseen-tensor

$$\mathbf{H}_{ij}^O = \frac{R}{r_{ij}} \left(\mathbf{I} + \frac{\mathbf{r}_{ij} \otimes \mathbf{r}_{ij}}{r_{ij}^2} \right). \tag{53}$$

Here R is the particle radius, $\mathbf{I}$ is the unity matrix and $\mathbf{r}_{\mathrm{ij}}$ is the distance vector $\mathbf{r}_{ij} = \mathbf{r}_j - \mathbf{r}_i$. The Oseen-tensor is the fundamental solution of the Stokes equation describing the flow field $\mathbf{v}_F(r)$ around a sphere of radius R dragged by an external force through the fluid. It describes the resulting fluid flow correctly at large distances $r \gg R$.

A hydrodynamic coupling of active Brownian particles was first introduced by Erdmann & Ebeling [28] using the Oseen-tensor. In their approach the point forces $\mathbf{f}_j$ correspond to the particle velocities $\mathbf{v}_j$. The resulting hydrodynamic velocity-alignment force reads

$$\mathbf{F}_{\mathrm{va}} = \chi_H \sum_j \mathbf{H}_{ij}^O \mathbf{v}_j = \chi_H \sum_j \frac{R}{r_{ij}} \left[\mathbf{I} + \frac{\mathbf{r}_{ij} \otimes \mathbf{r}_{ij}}{\mathbf{r}_{ij}^2} \right] \mathbf{v}_j. \tag{54}$$

In general a complex self-propelled object such as an bacterium is described by a force-multipole instead of a point force $\mathbf{f}_i$. The corresponding flow field can be obtained by a superposition of individual Oseen-flows (52). From detailed considerations of self-propelled swimmers at low Reynolds numbers it was shown that the first order terms of the resulting flow field $\mathbf{v}_F$ vanish. Thus the far field behaviour of the induced flow is dominated by a r^{-2}-term leading to a corresponding spatial dependence of the hydrodynamic coupling [29,30].

From the symmetry properties of the hydrodynamic tensor (53) it is obvious that the hydrodynamic interaction has a parallel component leading to an alignment of individual particle velocities. Therefore in terms of velocity alignment both interactions, (51) and (54), lead to similar dynamics (see also [31]). The main difference is the range: Whereas the velocity coupling in Eq. (51) is a strictly short-range interaction, the amplitude of the hydrodynamic coupling (54) decreases with $r^{-\alpha}$, where α represents the first non-vanishing order of the fluid velocity expansion.

From the biological point of view it seems, that for swarming bacteria the hydrodynamic interaction plays a minor role compared to direct coupling by massive flagellation [10]. Therefore we include the velocity alignment force into our model as introduced in Eq. (51).

The calculation method of the interaction is similar to the well-known Vicsek-model of self-propelled particles and was first introduced by Czirók et al. [9] into a microscopic model for bacterial dynamics.

The introduction of the velocity alignment interaction leads to novel dynamical behavior of chemotactic particle clusters [32]. For sufficiently large coupling strength χ the particles are able to correlate their velocities on the scale of several interaction radii ε. Depending on the parameters we observe either collective rotation or collective translation of a cluster (see Fig. 5).

In order to analyze the impact on the velocity-alignment interaction $\mathbf{F}_{\mathrm{va}}$ in a more qualitative way we performed simulations of a single chemotactic cluster of particles for different values of χ.

The chemotaxis parameters κ_0, β and the chemoattractant decay d_c were set arbitrarily to obtain a stable cluster with dimensions larger than the interaction range of the velocity alignment force ε.

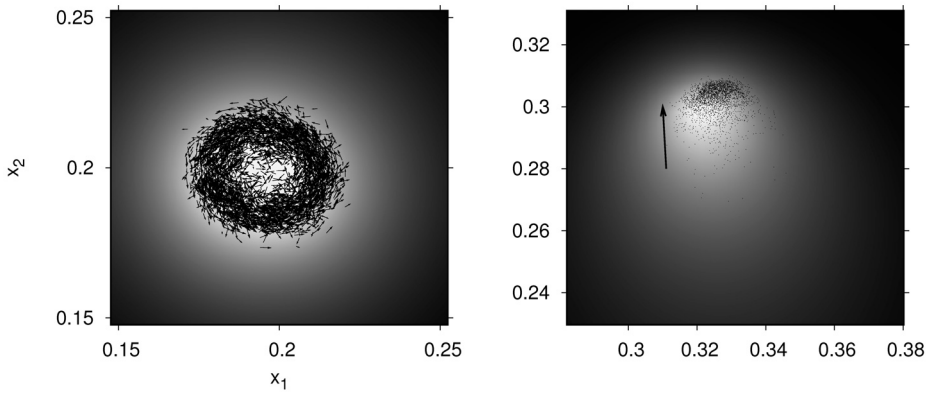

Fig. 5. Left: collective rotation of a chemotactic cluster of particles with velocity alignment for $\chi = 1.2\ \mathrm{s}^{-1}$. The position and the velocity of each individual particles is indicated by a vector. The background indicates the chemoattractant concentration c (bright for high and dark for low concentration). Right: for large coupling strength ($\chi = 2.6\ \mathrm{s}^{-1}$) the rotational motion breaks down and the entire cluster starts to move. For clarity only the positions of individual particles are shown as points together with the mean velocity. (Simulation parameters: $\kappa_0 = 8 \times 10^{-6}\ \mathrm{mm}^4\mathrm{s}^{-2}$, $\beta = 1 \times 10^{-3}\ \mathrm{mm}^2$, $d_c = 0.5\ \mathrm{s}^{-1}$, $\varepsilon = 1.17 \times 10^{-3}$ mm, $N = 3000$.)

We quantify rotational and parallel motion in terms of suitable order parameters. A convenient measure of collective rotation is the normalized angular momentum $\langle L \rangle$:

$$\langle L \rangle = \frac{1}{N} \left| \sum_{i=1}^{N} \frac{(\mathbf{x}_i - \mathbf{R}) \times \mathbf{v}_i}{|(\mathbf{r}_i - \mathbf{R})||\mathbf{v}_i|} \right|, \tag{55}$$

where $\mathbf{x}_i$ and $\mathbf{v}_i$ are the position and the velocity of the i-th particle and $\mathbf{R}$ is the center of mass vector. The angular momentum $\langle L \rangle$ is equal to 1, if all particles move on an ideal circular trajectory around the center of mass, and goes to zero in the absence of collective rotation.

The corresponding measure of the collective translation $\langle C_{\mathrm{vv}} \rangle$ is given by:

$$\langle C_{\mathrm{vv}} \rangle = \frac{1}{N^2} \sum_{i=1}^{N} \sum_{j=1}^{N} \frac{\mathbf{v}_i \mathbf{v}_j}{|\mathbf{v}_i||\mathbf{v}_j|}. \tag{56}$$

$\langle C_{\mathrm{vv}} \rangle$ is equal to 1 if all particle move in the same direction and vanishes for disordered motion.

We measured the two order parameters of motion in our simulations for a range of values of χ. To obtain a better statistics we took the time average of the respective parameter after the system reached its stationary state. The results of the simulation are summarized in Fig. 6.

For small χ, random noise dominates over the velocity alignment interaction and we basically observe a chemotactic cluster of particles with uncorrelated dynamics – both order parameters of motion, $\langle L \rangle$ and $\langle C_{\mathrm{vv}} \rangle$, vanish. If χ is increased further, the velocity alignment force F_{va} outweighs the stochastic force F^{s} acting on an individual particle, but is still weaker than the chemotactic force F_{ch}. This situation leads to collective rotational motion, as the particles correlate their dynamics on the microscopic level but are confined by the chemoattractant field (see Fig. 5). A further increase of χ results in a breakdown of the rotational motion. The particles are able to escape collectively out of the self-generated maximum of the chemoattractant field. As the particles keep on producing the chemoattractant, they drag a cloud of chemoattractant around them and we observe a compact chemically bounded cluster of bacteria performing collective translation as in Fig. 5. The transition from collective rotation to collective translation goes along with a significant collapse of the cluster and unbiologically large densities of particles. The reason is that we neglect the finite size of bacteria and the resulting volume exclusion in our model. Nevertheless we expect similar behavior in more realistic model.

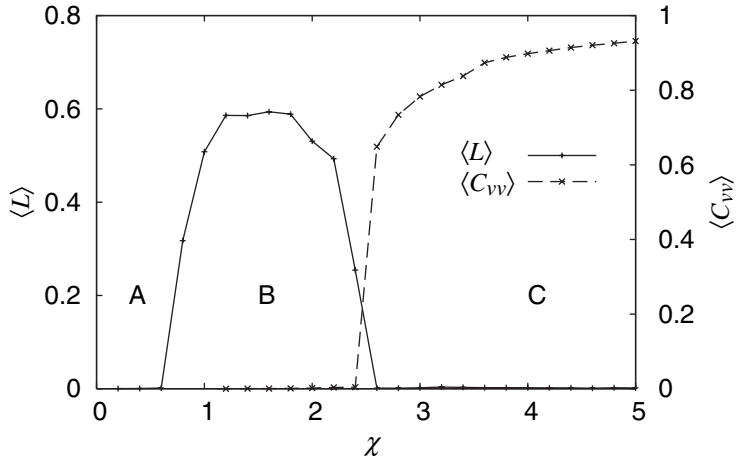

Fig. 6. The rotational motion $\langle L \rangle$ (55) and parallel motion $\langle C_{\mathrm{vv}} \rangle$ (56) order parameters for an individual cluster of particles over the velocity-alignment strength χ. Depending on χ three different states can be identified: (A) no collective mode of motion; (B) collective rotation; (C) collective translation. (Simulation parameters: $\kappa_0 = 1 \times 10^{-5}$ mm^{4}s^{-2}, $\beta = 6 \times 10^{-5}$ mm^2, $d_c = 0.1$ s^{-1}, $D = 1 \times 10^{-4}$mm^{2}s, $N = 3000$ and $l_{va} = 2 \times 10^{-3}$ mm.)

Collective rotation of bacterial clusters has been reported and modelled by Czirók et al. [9]. Czirók et al. explain rotating structures in terms of an additional interaction, the so-called rotational chemotaxis. This additional interaction leads intrinsically by its mathematical formulation to rotating structures. From the above results it can be concluded that the additional introduction of rotational chemotaxis is redundant and that the collective rotational behavior of particles can be explained simply in terms of confined self-propelled particles with velocity alignment. In case of bacteria this confinement originates from the chemical cell to cell signaling via the self-generated chemoattractant, as in our approach. Additionally we imply that the active Brownian particle model is also able to explain the occurrence of collective translation motion enhanced by chemotaxis as presented by Soni et al. [33].

Concluding these section we suggest, based on the presented results, a simple explanation for rotating, as well as, moving bacterial clusters: Both modes of motion origin from the complex interaction of velocity alignment and chemotaxis. The force ratio f of these two interactions determines the mode of motion of a bacterial cluster and we would expect it should be possible to test this hypothesis through careful experiments on swarming, chemotactic bacteria in which one of the forces is artificially modified.

6 Conclusion and discussion

In this work we propose a minimal model for bacterial colonies based on the concept of active Brownian particles. This individual based approach allows the description of macroscopic colony patterns, mesoscopic collective dynamics, as well as, microscopic behavior of individual cells by a single mathematical model. From review of the experimental data on bacteria (*E. coli*) we are able to reduce the number of free parameters and analyze the occurring dynamics in dependence on the remaining parameters.

By neglecting the active motility we derived a mean-field description in terms of partial differential equations for the bacterial density ρ and the chemoattractant concentration c. The mean field description represents a variant of the well known Keller-Segel-model. The comparison of the results of mean-field approximation with the microscopic model suggests that in case of bacteria interacting only via chemical cell-to-cell signaling the active motility does not significantly alter the macroscopic dynamics.

On the microscopic level the individual cell dynamics are uncorrelated and each bacterium performs complex rotational motion in an effective chemotactic potential. The dynamics within

such a stationary chemotactic cluster can be approximated by a self-propelled motion in a parabolic potential.

In order to account for the observed swarming motility of bacteria, we extended the model by an additional velocity alignment interaction. In dependence on the strength of the velocity alignment coupling two different modes of collective motion of chemotactic clusters can be observed: For intermediate coupling strength we observe collective rotation of within the clusters. For stronger coupling the rotational motion breaks down and we observe collective translation of entire clusters.

Concluding it has to be pointed out that the active Brownian particle model of bacterial colonies is — in spite of its complexity and rich dynamics — still a rather minimalistic description of bacterial colonies. In the formulation of our model we did not take into account the finite size of bacteria and their shape [34]. One consequence is the possibility of unrealistic high cell densities.

Individual based models of bacterial dynamics in general, and the here presented ABP-model in particular, are in our opinion the natural description of bacterial colonies. They have several advantages in comparison with the widely employed mean field models. Among others they

- are easier to handle numerically,
- allow simulations at low densities where the mean field approach gets questionable, and
- allow easy extension of the model to non-identical particles.

But the most important ability of the models is the natural realization of the active motility of bacteria, which is the only possibility to account for a large part of dynamics observed in bacterial colonies.

References

1. E.F. Keller, L.A. Segel, J. Theor. Biol. **30**, 225 (1971)
2. E.F. Keller, L.A. Segel, J. Theor. Biol. **30**, 235 (1971)
3. R. Tyson, S.R. Lubkin, J.D. Murray, J. Math. Biol. **38**, 359 (1999)
4. R. Tyson, S.R. Lubkin, J.D Murray, Proc. Royal Soc. London B **266**, 299 (1999)
5. M. Matsushita, J. Wakita, H. Itoh, K. Watanabe, T. Arai, T. Matsuyama, H. Sakaguchi, M. Mimura, Physica A **274**, 190 (1999)
6. Y. Kozlovsky, I. Cohen, I. Golding, E. Ben-Jacob, Phys. Rev. E **59**, 7025 (1999)
7. E.O. Budrene, H.C. Berg, Nature **349**, 630 (1991)
8. E.O. Budrene, H.C. Berg, Nature **376**, 49 (1995)
9. A. Czirók, E. Ben-Jacob, I. Cohen, T. Vicsek, Phys. Rev. E **54**, 1791 (1996)
10. M. Eisenbach, *Chemotaxis* (World Scientific Publishing, 2004)
11. W. Ebeling, F. Schweitzer, B. Tilch, BioSystems **49**, 17 (1999)
12. U. Erdmann, W. Ebeling, L. Schimansky-Geier, F. Schweitzer, Eur. Phys. J. B **15**, 105 (2000)
13. U. Erdmann, W. Ebeling, V.S. Anishchenko, Phys. Rev. E **65**, 061106 (2002)
14. W. Ebeling, Physica A **314**, 92 (2002)
15. B.A. Mello, L. Shaw, Y. Tu, Biophys. J. **87**, 1578 (2004)
16. S.-H. Kim, W. Wang, K.K. Kim, Proc. Nation. Acad. Sci. USA **99**, 11611 (2002)
17. V. Sourjik, H.C. Berg, Proc. Nation. Acad. Sci. USA **99**, 123 (2002)
18. E. Ben-Jacob, I. Cohen, H. Levine, Adv. Phys. **49**, 395 (2000)
19. J.D. Murray, *Mathematical Biology I*, 3 edn. (Springer, Berlin, 2004)
20. F. Schweitzer, L. Schimansky-Geier, Physica A **206**, 359 (1994)
21. A.S. Mikhailov, D. Meinköhn, *Self-motion in physico-chemical systems far from equilibrium*, Vol. 484, Lecture Notes in Physics (Springer-Verlag, Berlin, 1997), p. 334
22. M. Loferer-Krösbacher, J. Klima, R. Psenner, Appl. Envir. Microbiol. **64**, 688 (1997)
23. A. Czirók, T. Vicsek, Physica A **281**, 17 (2000)
24. M.R. D'Orsogna, Y.L. Chuang, A.L. Bertozzi, L.S. Chayes, Phys. Rev. Lett. **96**, 104302 (2006)
25. U. Erdmann, W. Ebeling, L. Schimansky-Geier, F. Schweitzer, Eur. Phys. J. B, **15**, 105 (2000)
26. L. Schimansky-Geier, W. Ebeling, U. Erdmann, Acta Phys. Polon. **36**, 1757 (2005)
27. W.Q. Zhu, M. Lin Deng, Phys. A: Stat. Mech. Appl. **354**, 127 (2005)

28. U. Erdmann, W. Ebeling, Fluc. Noise Lett. **3**, 145 (2003)
29. T.J. Pedley, J.O. Kessler, Ann. Rev. Fluid Mech. **24**, 313 (1992)
30. C.M. Pooley, G.P. Alexander, J.M Yeomans, Swimming with a friend at low reynolds number, 0705.3612 (2007)
31. Z. Csahók, A. Czirók, Physica A **243**, 304 (1997)
32. P. Romanczuk, U. Erdmann, PRL (2007) (submitted)
33. G.V. Soni, B.M. Jaffar Ali, Y. Hatwalne, G.V. Shivashankar, Biophys. J. **84**, 2634 (2003)
34. F. Peruani, A. Deutsch, M. Bar, Phys. Rev. E (Stat. Nonl. Soft Matter Phys.) **74**, 030904–4 (2006)